THE JOURNAL OF PHYSICAL CHEMISTRY C

Article

Magnetic Interactions and Energy Barrier Enhancement in Core/Shell Bimagnetic Nanoparticles

Gabriel Carlos Lavorato, Davide Peddis, Enio Lima, Jr., Horacio E. Troiani, Elisabetta Agostinelli, Dino Fiorani, Roberto Daniel Zysler, and Elin Lilian Winkler

J. Phys. Chem. C, **Just Accepted Manuscript** • DOI: 10.1021/acs.jpcc.5b04448 • Publication Date (Web): 11 Jun 2015

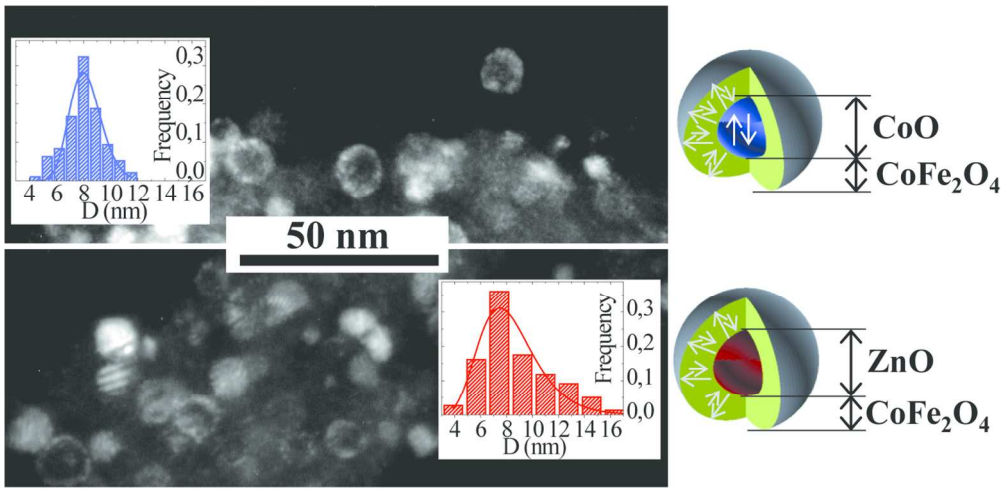

Dark-field TEM micrographs of $CoO/CoFe_2O_4$ (upper panel) and $ZnO/CoFe_2O_4$ (bottom panel) and a schematic representation of the core/shell structures. Inset: size distributions of $CoO/CoFe_2O_4$ and $ZnO/CoFe_2O_4$ nanoparticles.
126x62mm (300 x 300 DPI)

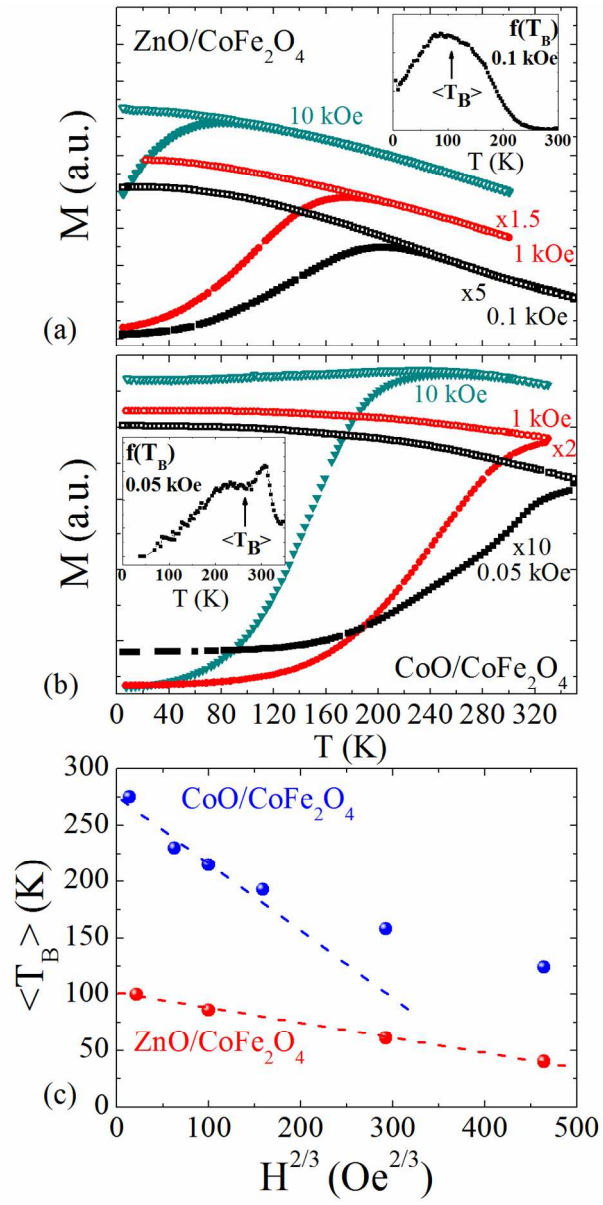

Temperature dependence of magnetization for (a) $ZnO/CoFe_2O_4$ nanoparticles (b) $CoO/CoFe_2O_4$ nanoparticles (full symbols indicate ZFC curves and empty symbols indicate FC curves, for clarity the curves were scaled by a fixed factor). (c) Mean blocking temperature as a function of the applied field (dashed lines are a guide to the eye).
84x167mm (300 x 300 DPI)

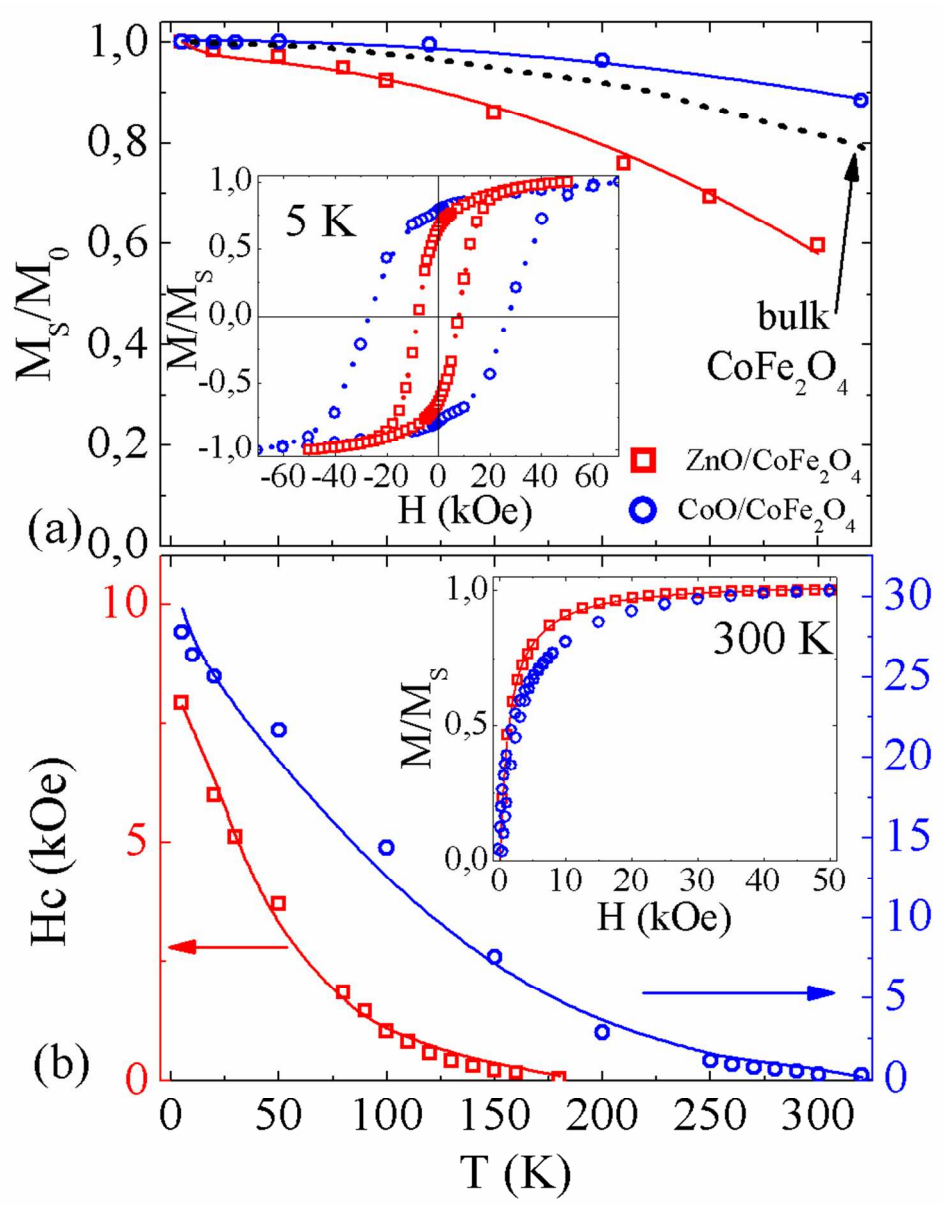

(a) Temperature dependence of the saturation magnetization ratio M_S/M_0 for $ZnO/CoFe_2O_4$ and $CoO/CoFe_2O_4$ nanoparticles (bulk $CoFe_2O_4$ experimental values from ref 41 are shown for comparison). Inset: Hysteresis loops at 5 K. (b) Temperature dependence of the coercive field. Inset: field dependence of magnetization at 300 K. (full lines represent the corresponding fits).
84x107mm (300 x 300 DPI)

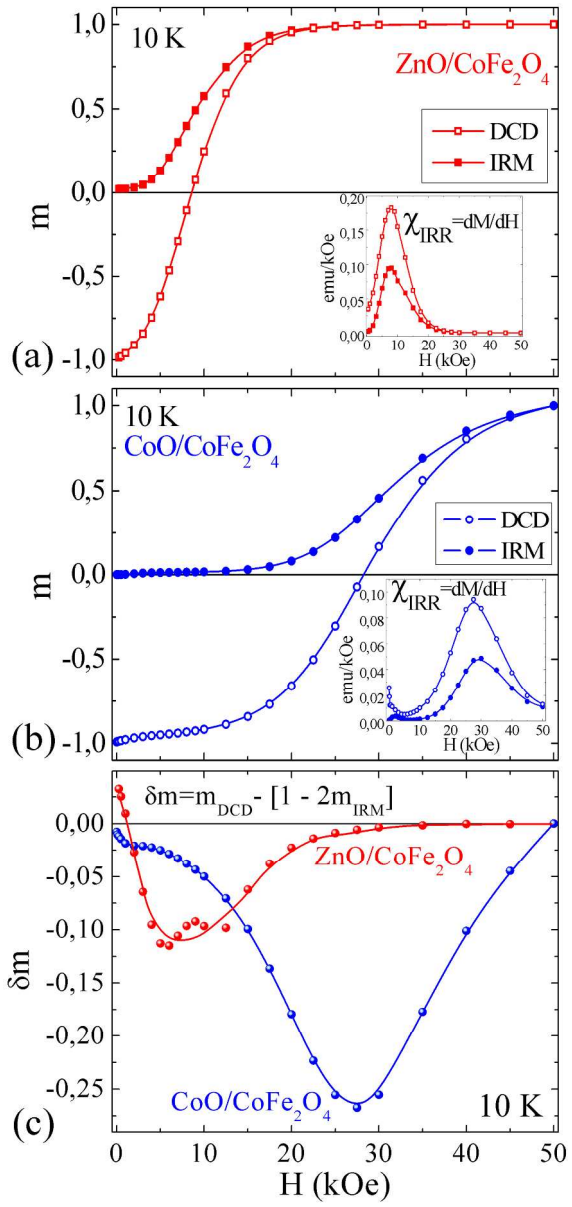

DCD (empty symbols) and IRM (full symbols) curves for (a) $ZnO/CoFe_2O_4$ nanoparticles and (b) $CoO/CoFe_2O_4$ nanoparticles measured at 10 K. (c) δm plots and (insets) irreversible susceptibilities calculated from the DCD and IRM curves (lines are a guide to the eye).
172x353mm (300 x 300 DPI)

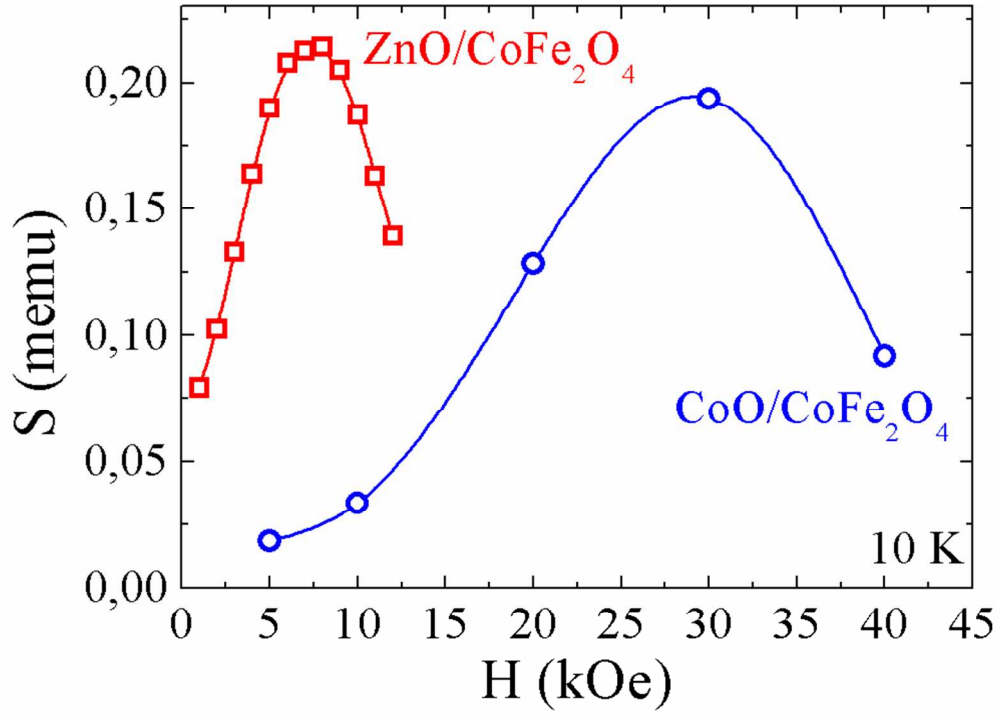

Magnetic viscosity coefficient (S) as a function of the reverse field for $ZnO/CoFe_2O_4$ and $CoO/CoFe_2O_4$ nanoparticles (lines are a guide to the eye).
84x59mm (300 x 300 DPI)

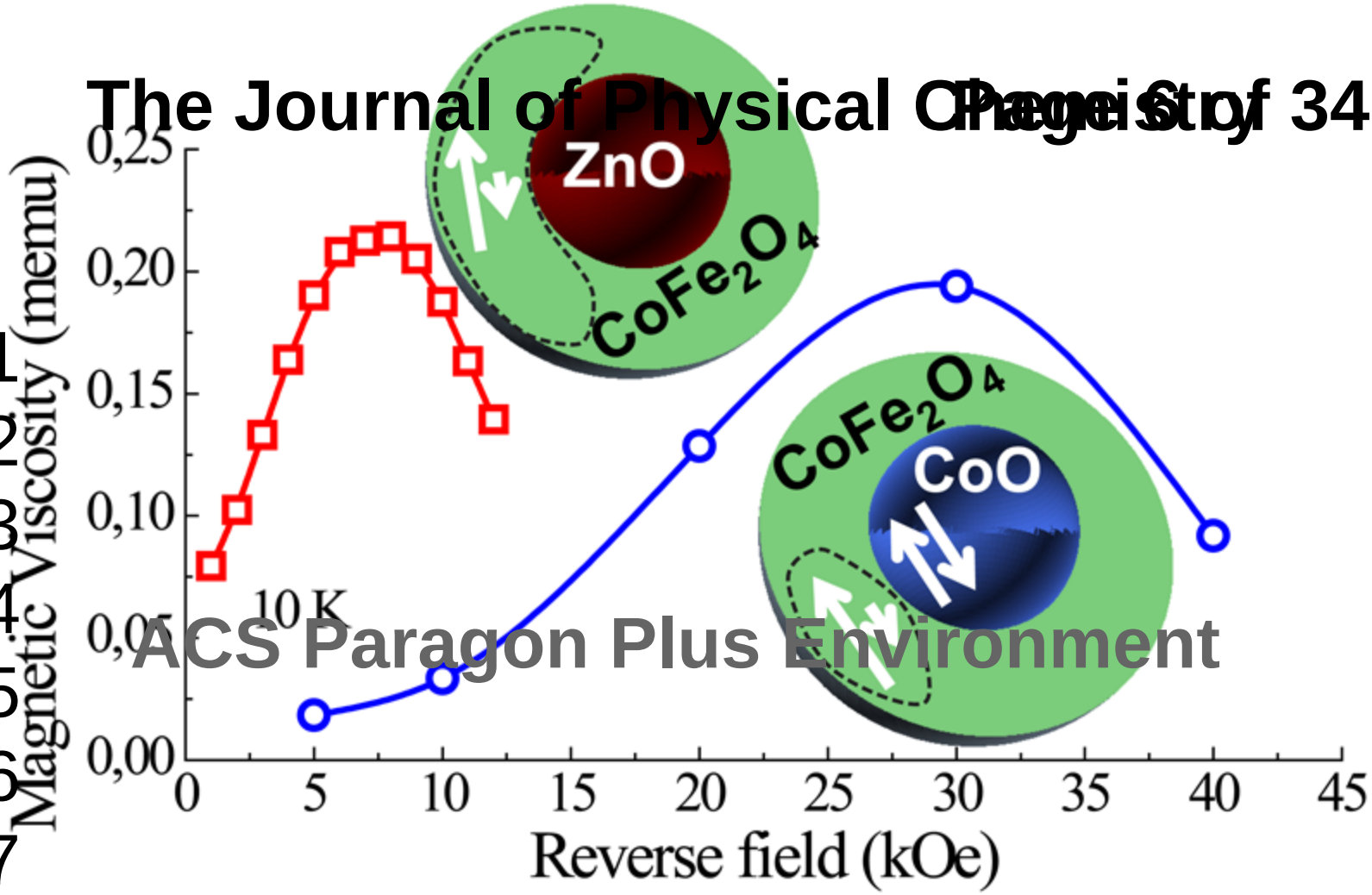

Magnetic Interactions and Energy Barrier Enhancement in Core/Shell Bimagnetic Nanoparticles

Gabriel C. Lavorato[†,§], Davide Peddis[‡,§], Enio Lima Jr[†,§], Horacio E. Troiani[†], Elisabetta Agostinelli[‡,§], Dino Fiorani[‡,§], Roberto D. Zysler[†,§], Elin L. Winkler[†,§,]*

† Centro Atómico Bariloche and CONICET, 8400 S.C. de Bariloche, RN, Argentina.

‡ Istituto di Struttura della materia-CNR, Area della Ricerca di Roma, Po.Box 10, I-00015 Monterotondo (Roma), Italy.

§ Argentine-Italian Joint Laboratory of Nanomagnetism, LIANAM, Laboratorio Resonancias Magnéticas−CNEA, Argentina/ Istituto di Struttura della Materia, CNR, Italy.

ABSTRACT

In this work we studied the dynamic and static magnetic properties of ZnO-core/$CoFe_2O_4$-shell and CoO-core/$CoFe_2O_4$-shell nanoparticles. Both systems are formed by a core of ~ 4 nm of diameter encapsulated in a shell of ~ 2 nm of thickness. The mean blocking temperature changes from 106(7) K to 276(5) K when the core is diamagnetic or antiferromagnetic, respectively. Magnetic remanence studies revealed the presence of

weak dipolar inter-particle interactions, where H_{int} is approximately - 0.1 kOe for $ZnO/CoFe_2O_4$ and - 0.9 kOe for $CoO/CoFe_2O_4$, playing a minor role in the magnetic behavior of the materials. Relaxation experiments provided evidence that the magnetization reversal process of $CoFe_2O_4$ is strongly dependent on the magnetic order of the core. At 10 K, activation volumes of ~ 46(6) and ~ 69(5) nm^3 were found for $CoO/CoFe_2O_4$ and $ZnO/CoFe_2O_4$ nanoparticles, respectively, corresponding to one-third and one-fifth of the total shell volume. While the magnetic behavior of $ZnO/CoFe_2O_4$ nanoparticles is strongly affected by the surface disorder, the exchange coupling at the $CoO/CoFe_2O_4$ interface rules the magnetization reversal and the nanoparticles' thermal stability by inducing a larger energy barrier and promoting smaller switching volume.

KEYWORDS: Magnetic Nanoparticles, Exchange-coupling, Magnetic anisotropy, Interparticle interactions, Intraparticle interactions, Cobalt ferrite.

1. INTRODUCTION

The search for new magnetic materials has motivated the fabrication and study of nanostructures with tuned and improved properties that would allow the development of novel and promising technologies. Among nanostructured materials, magnetic nanoparticles (NPs) attract great interest because they can be applied in different fields as data storage,[1–4] permanent magnets,[5–8] optics,[9] catalysis[10] and nanomedicine.[11,12] In particular, the possibility of fabricating bimagnetic NPs, that combine materials with different magnetic order and anisotropy, has added a new degree of freedom to better tune specific properties.[13–17] The progress in the production of advanced magnetic NPs is based on the synergy between new fabrication techniques and the understanding of the origin of the interactions governing the magnetic behavior. A number of bimagnetic

antiferromagnetic (AFM)/ferrimagnetic (FiM) interface exchange-coupled core/shell systems have shown improved properties such as an increase of the coercive field (H_C) and thermal stability[18] and high and tunable exchange bias fields (H_{EB}).[19,20] However, the complexity of these nanostructures adds new factors, *e.g.* inter and intra-particle interactions, shape, surface and/or magnetocrystalline anisotropy, size distribution, that make more difficult the analysis. The mentioned factors directly affect the energy barrier distribution and, as a consequence, they alter the magnetization reversal process and determine the range of application of a particular magnetic material.

In this work we studied the influence of the interface exchange interaction on the magnetization reversal process by comparing two bimagnetic nanoparticle systems with analogous size and morphology. One system is formed by NPs with a diamagnetic ZnO core encapsulated in a FiM $CoFe_2O_4$ shell while the other one consists of NPs with an AFM CoO core encapsulated in a FiM $CoFe_2O_4$ shell. The energy barrier distribution of ZnO/$CoFe_2O_4$ system is expected to be determined by size, shape and distribution of magnetic anisotropy, but may also be modified by the inter-particle interactions. For the CoO/$CoFe_2O_4$ system, besides the previously mentioned contributions to the energy barrier distribution, intra-particle interactions due to the exchange interaction at the AFM/FiM interface could play a relevant role in the NPs' magnetic moment reversal. The samples were studied through various conventional DC magnetization measurements with the aim of determining the energy barrier distributions and how they are affected by inter- and intra-particle interactions. In addition, the magnetic viscosity, originated by the thermally activated transition over the energy barrier, and the activation volume, defined when the system overcomes the energy maximum, were analyzed taking into account their correlation with surface effects and magnetic interactions.

2. SAMPLE PREPARATION AND EXPERIMENTAL SETUP

ZnO core/ $CoFe_2O_4$ shell and CoO core/ $CoFe_2O_4$ shell nanoparticles were synthesized by combining the chemical route of high temperature decomposition of organometallic precursors with a seed-mediated process.[21,22] A detailed description of the synthesis is reported in ref 23. To fabricate ZnO NPs, 3 mmol Zn(II) acetylacetonate ($Zn(acac)_2$) were mixed with long-chain alcohol 1-2 octanediol (1.8 mmol), diphenyl ether (190 mmol), oleic acid (9 mmol) and oleylamine (9 mmol) and heated up to T ~ 260 ºC for 120 min. The $CoFe_2O_4$ was overgrown by adding $Co(acac)_2$ and $Fe(acac)_3$ with 1:2 molar ratio (0.6:1.2 mmol) together with 1-2 octanediol (2 10^{-2} mmol), diphenyl ether (95 mmol), oleic acid (3 mmol) and oleylamine (3 mmol). The solution was magnetically stirred and heated up to the boiling temperature T ~ 260 ºC for 120 min. After cooling down to room temperature, the NPs were washed several times with a mix of ethanol and toluene 10:1 solution. In order to improve the sample crystallinity,[24] the obtained dry powder was annealed at T ~ 300 ºC in air atmosphere for 2 h. Afterwards, the sample was re-dispersed in ethanol and the suspension was dropped on a copper grid for transmission electron microscopy (TEM) observation. The morphology and particle size were evaluated in a Philips CM200 UT TEM microscope operating at 200 kV by measuring around 300 particles of each sample in either bright-field and dark-field micrographs. The DC magnetization measurements were performed by a Quantum Design SQUID magnetometer, equipped with a superconducting coil that produces magnetic fields in the range ± 50 kOe. Samples in the form of powders were immobilized in an epoxy resin to prevent any movement of the NPs during the measurements. Magnetization versus temperature measurements were performed using

zero-field-cooled (ZFC) and field-cooled (FC) protocols. ZFC and FC magnetization measurements were carried out by cooling the sample from room temperature to 5 K in zero magnetic field, then, a static magnetic field was applied. M_{ZFC} was measured during the warm-up from 5 K to 300 K, whereas M_{FC} was recorded during the subsequent cooling-down. The field dependence of remanent magnetization was measured using the isothermal remanent magnetization (IRM) and direct current demagnetization (DCD) protocols. The initial state for an IRM measurement is a totally demagnetized sample cooled in zero magnetic field. In the present case, an external field was applied and kept for 10 s; then, it was switched off and the remanence was measured (M_{IRM}). The process was repeated increasing the field up to saturation. In a DCD measurement, the initial state is the magnetically saturated one. An external field of 50 kOe was applied and kept for 10 s; then, a small external field in the direction opposite to magnetization was applied and, after 10 s, it was switched off and the remanent magnetization (M_{DCD}) was measured. This was repeated while increasing the field up to + 50 kOe. The time dependence of magnetization was investigated by saturating the samples with a 50 kOe applied field and then measuring the magnetization after the application of reverse fields with different magnitude and values close to the coercivity of each sample.

3. EXPERIMENTAL RESULTS AND DISCUSSION

3.1 Structural Characterization

TEM images evidence that the samples are composed by ZnO NPs (or CoO NPs) encapsulated in $CoFe_2O_4$. The samples consist of ~ 8 nm NPs formed by ~ 4 nm diameter ZnO (or CoO) cores surrounded by a ~ 2 nm thick cobalt ferrite shell (as detailed in Table 1). The inset of Figure 1 shows the NPs' size dispersion, obtained from TEM

measurements, where a log-normal distribution is observed for both systems. Characteristic dark-field TEM micrographs, obtained by the intensity of a fraction of $CoFe_2O_4$ (111) diffraction ring, evidence the core/shell morphology of the material (Figure 1); for clarity, a schematic representation of the NPs' architecture is also reported. A comprehensive structural characterization is reported elsewhere.[23]

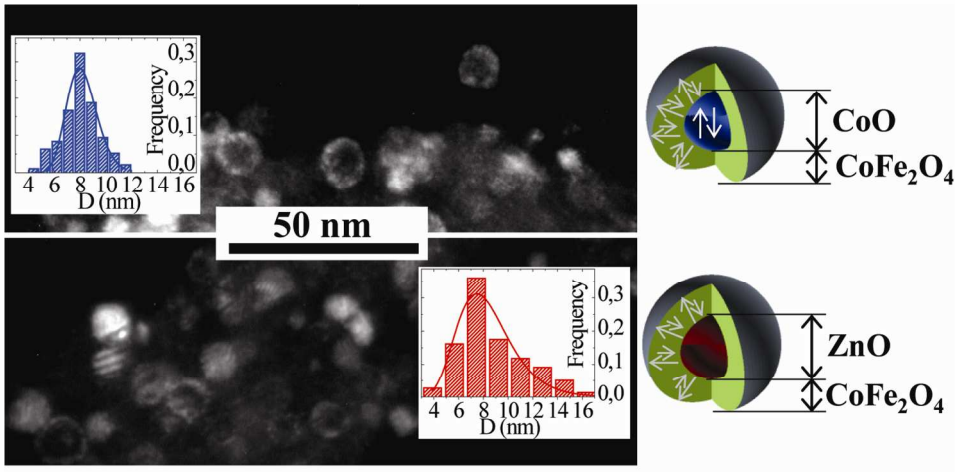

Figure 1 Dark-field TEM micrographs of $CoO/CoFe_2O_4$ (upper panel) and $ZnO/CoFe_2O_4$ (bottom panel) and a schematic representation of the core/shell structures. Inset: size distributions of $CoO/CoFe_2O_4$ and $ZnO/CoFe_2O_4$ nanoparticles.

3.2 Magnetic Behavior

Magnetization versus temperature curves were measured following ZFC and FC protocols at applied fields in the range 0.05-20 kOe (see Figure 2 and Figure S1 at the supporting information). The ZFC and FC magnetization measurements suggest the presence of a blocking process typical of an assembly of magnetic NPs with a distribution of blocking temperatures (T_B). The maximum of the low-field ZFC curve is located at ~ 200 K for $ZnO/CoFe_2O_4$ NPs and above room temperature for the $CoO/CoFe_2O_4$ system when the measurement is performed at 0.1 kOe and 0.05 kOe respectively, and both shift

toward lower temperatures when the measurement is performed applying higher magnetic fields. In addition, the FC curves of both samples show a weak temperature dependence below the ZFC maximum, suggesting the presence of magnetic interactions.

In order to quantify the dependence of T_B on the magnetic field we refer to the Néel model for an assembly of identical non-interacting single domain NPs. Within this model T_B can be defined as the temperature where the relaxation time (τ) is equal to the experimental "time window" (τ_m): $T_B = \frac{\Delta E}{\ln(\tau_m/\tau)k_B}$, where ΔE corresponds to the energy barrier and k_B is the Boltzmann constant. However, real particle systems present interactions and a distribution of size and magnetic anisotropy that simultaneously affect the energy barrier. The irreversibility between ZFC and FC curves arises from the distribution of energy barriers or blocking temperatures $f(T_B)$, therefore the mentioned T_B distribution could be determined through the relation $f(T_B) \sim (1/T)d(M_{ZFC} - M_{FC})/dT$,[25–27] and the mean blocking temperature, $\langle T_B \rangle$, can be defined as follows:

$$\langle T_B \rangle = \frac{\int_0^\infty T_B f(T_B) dT_B}{\int_0^\infty f(T_B) dT_B} \qquad \text{(Equation 1)}$$

The insets of Figures 2a-b show $f(T_B)$ calculated from the low-field ZFC and FC magnetization curves. It is important to notice that the size distributions obtained from TEM measurements show typical log-normal size distributions with a single peak for both systems (see insets of Figure 1). However, while the $f(T_B)$ curve for ZnO/$CoFe_2O_4$ particles also shows a lognormal temperature dependence with a single maximum, the bimagnetic CoO/$CoFe_2O_4$ system presents two relative maxima located at ~230 K and ~290 K. These results evidence that the CoO/$CoFe_2O_4$ system presents other contributions to the energy barrier, in addition to the size dispersion. In particular, the high temperature

anomaly is still observed at higher applied fields (as shown in Figure S2 at the supporting information) and its position matches well with the Néel temperature of CoO (T_N ~290 K). The mean blocking temperature, $\langle T_B \rangle$, calculated at low fields from Equation 1, changes from $\langle T_B \rangle = 106(7)\,K$ to $\langle T_B \rangle = 276(5)\,K$ when the core is diamagnetic or AFM, respectively. Such significant difference implies an enhancement of the thermal stability of $CoO/CoFe_2O_4$ system ascribed to the presence of interface exchange interaction.

The magnetic field dependence of the magnetization reversal process is usually analyzed through the relation $\langle T_B \rangle(H) = T_0[1 - (H/H_0)^{2/3}]$ obtained for single domain NPs, where H_0 and T_0 are the coercive field at zero temperature and the blocking temperature at zero field, respectively.[25,28–30] Figure 2c presents $\langle T_B \rangle$ as a function of $H^{2/3}$: while $ZnO/CoFe_2O_4$ NPs present a linear trend, as expected for non-interacting particles,[25,31] for $CoO/CoFe_2O_4$ NPs the variation does not follow the $H^{2/3}$ dependence. Such discrepancy suggests that for $CoO/CoFe_2O_4$ NPs both magnetic intra-particle and/or inter-particle interactions are playing a major role in determining the energy barrier.

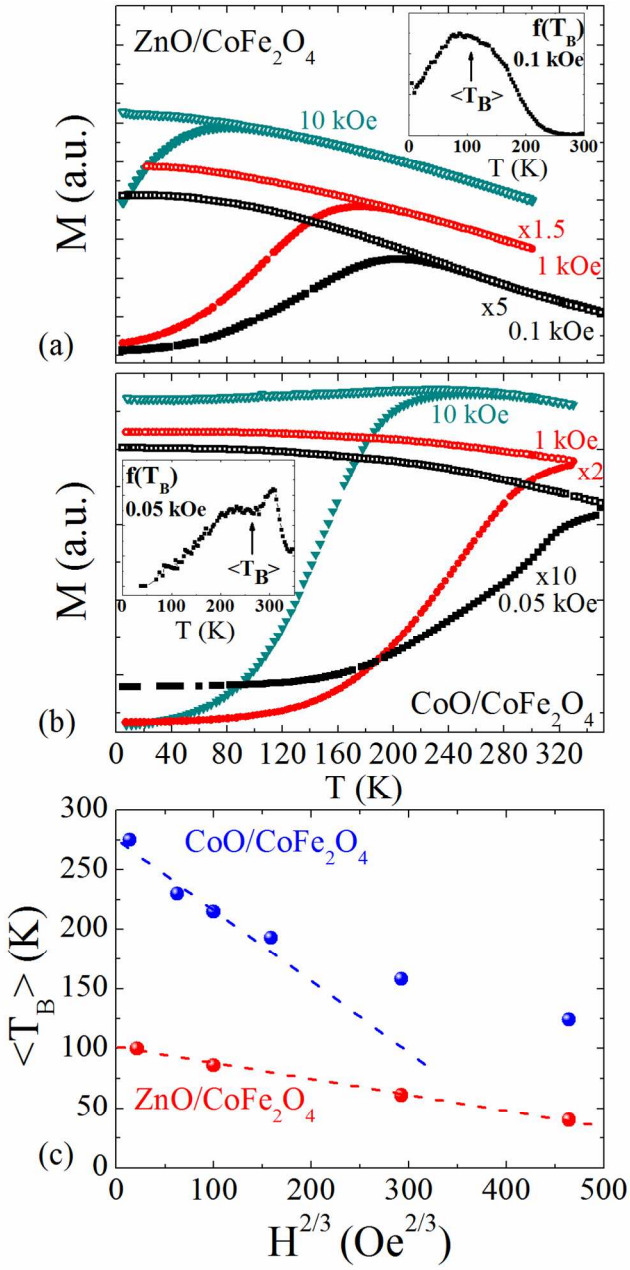

Figure 2 Temperature dependence of magnetization for (a) $ZnO/CoFe_2O_4$ nanoparticles (b) $CoO/CoFe_2O_4$ nanoparticles (full symbols indicate ZFC curves and empty symbols indicate FC curves, for clarity the curves were scaled by a fixed factor). (c) Mean blocking temperature as a function of the applied field (dashed lines are a guide to the eye).

Table 1 Summary of the characterization parameters: mean diameter $\langle D \rangle$ and diameter dispersion (σ_D) from TEM measurements, coercive field at 5K (H_C 5K), mean blocking temperature $\langle T_B \rangle$, inter-particle interaction field estimated from remanence studies at 10 K (H_{int} 10 K) and activation volume calculated from relaxation and remanence measurements at 10 K (V_{ACT} 10 K).

Sample	$\langle D \rangle$ (nm)	σ_D (nm)	H_C 5K (kOe)	$\langle T_B \rangle$ (K)	H_{int} 10 K (kOe)	V_{ACT} 10 K (nm^3)
$ZnO/CoFe_2O_4$	8.1	1.6	7.8(1)	106(7)	- 0.1(2)	69(5)
$CoO/CoFe_2O_4$	8.2	1.2	27.8(2)	276(5)	- 0.9(3)	46(6)

The field dependence of magnetization was measured at different temperatures for both samples. The insets of Figures 3a-b show the M(H) curves measured at 5 K and 300 K, respectively. The low temperature (5 K) hysteresis curve shows a remarkable increase of the coercive field when the core is AFM: H_C changes from 7.8(1) kOe to 27.8(2) kOe for $ZnO/CoFe_2O_4$ and $CoO/CoFe_2O_4$, respectively. Besides, at room temperature the magnetization of $ZnO/CoFe_2O_4$ NPs is fully reversible reflecting the superparamagnetic behavior of the sample. In this case, the magnetic volume at 300 K can be derived by fitting the experimental data with a Langevin function and a lognormal distribution for the magnetic moments.[32] A mean magnetic moment per particle of 2328(70) μ_B was estimated, which corresponds to an average magnetic volume of 46(3) nm^3 calculated from the $CoFe_2O_4$ bulk magnetic moment per unit formula and its lattice parameter.[33] Considering that the overall shell volume is 235 nm^3, such result implies that at room temperature the FiM shell is formed by several superparamagnetic clusters.

Figure 3a reports the temperature dependence of the saturation magnetization, $M_S(T)$, normalized to the saturation magnetization extrapolated at zero temperature (M_0). Both samples show a decrease of $M_S(T)/M_0$ when the temperature is raised, being this decay more pronounced for the ZnO/$CoFe_2O_4$ system, particularly in the low temperature range ($T < 50\ K$) where a sharp reduction of $M_S(T)$ is observed. The decrease of the magnetization with temperature in an ordered magnetic system is related to the low energy collective excitations or spin waves.[34] Such behavior can be analyzed through the modified Bloch expression given by

$$M_S(T)/M_0 = 1 - BT^{\alpha} + A_0 e^{-T/T_f} \qquad \text{(Equation 2)}$$

where α and B are parameters that depend on the characteristic of the magnetic system and the exponential term is a correction due the magnetically disordered layer that depends on the size of the particle through the fitting term A_0 and on a spin-glass freezing temperature given by T_f. While $\alpha = 3/2$ has been observed for many bulk materials, in nanostructured magnetic materials deviations from B_{bulk} and α_{bulk} are usually found.[34,35] Hendriksen *et al.* in ref 35 took into account size effects in calculating the temperature dependence of the magnetic moment based on a thermal distribution of spin waves and obtained a power law with $\alpha = 2$ and B similar to the bulk value. The mentioned work remarks that the parameter α is size dependent but structure independent; on the other hand, B is related to the effective coordination number of the magnetic cluster (mean number of nearest neighbors), where a larger B corresponds to "open" clusters with a lower coordination number for the surface ions. For $CoFe_2O_4$, bulk $\alpha = 2$ and $B \sim 1.6 \cdot 10^{-6}\ K^{-2}$ have been measured.[36,37] $B > B_{bulk}$ was found for small NPs and B approaches the bulk value when the NPs' size increases.[34,35] By fitting the data of Figure 3a with a fixed $\alpha = 2$

we have found that the exponential term is negligible for $CoO/CoFe_2O_4$ NPs but that it should be taken into account for the low temperature increase observed for $ZnO/CoFe_2O_4$, where $A_0 = 0.05$ and $T_f = 10\,K$ have been obtained. These results suggest that the $ZnO/CoFe_2O_4$ system presents a larger magnetically disordered surface, while for the $CoO/CoFe_2O_4$ NPs the AFM core promotes a higher degree of magnetic ordering of the FiM shell by the interface exchange interaction. Interestingly, while $B{\sim}4.5 \cdot 10^{-6}\,K^{-2}$ is higher than B_{bulk} for $ZnO/CoFe_2O_4$ (as expected for nanostructured materials with a reduced mean number of nearest neighbors), $B{\sim}1.1 \cdot 10^{-6}\,K^{-2}$ results even lower than B_{bulk} for $CoO/CoFe_2O_4$, highlighting the important effect of the exchange interaction at the AFM/FiM interface, which reduces the surface magnetic disorder by increasing the mean number of interacting nearest neighbors and enhances the magnetization thermal stability.

The temperature dependence of the coercive field for both systems is displayed in Figure 3b, where a monotonously decrease of H_C with temperature is observed and an almost four times larger H_C value for the $CoO/CoFe_2O_4$ system is found compared to $ZnO/CoFe_2O_4$. From the energy barrier, calculated for non-interacting and single-domain NPs in the presence of a magnetic field, the temperature dependence of H_C results[25]

$$H_C(T) = H_0\left(1 - \sqrt{T/T_B}\right) \qquad \text{(Equation 3)}$$

where the coercivity at the zero temperature limit, H_0, depends on the degree of alignment of the particles' easy axes. However, this well-known equation does not consider the size distribution and the intra- or inter-particle interactions that modify the energy barrier. The energy barrier distribution affects $H_C(T)$ because at a particular T only particles with $T_B > T$ will contribute to the hysteresis; thus, a correction could be taken

into account by replacing T_B in Equation 3 with a temperature dependent mean blocking temperature $\langle T_B \rangle_T$, defined as follows:[38]

$$\langle T_B \rangle_T = \frac{\int_T^\infty T_B f(T_B) dT_B}{\int_T^\infty f(T_B) dT_B} \qquad \text{(Equation 4)}$$

The coercive field where only the blocked particles are considered is called $H_{CB}(T)$ and is expected to follow the Equation 3 modified by $\langle T_B \rangle_T$. On the other hand, when the temperature raises the fraction of superparamagnetic particles increases and, as a consequence, the average coercive field is reduced. According to refs 38,39 the mean coercive field for a mixture of superparamagnetic and blocked particles, $\langle H_C \rangle_T$, can be calculated from the linear contribution of the superparamagnetic and blocked components of magnetization. Within this approximation, $\langle H_C \rangle_T$ results

$$\langle H_C \rangle_T = H_{CB}(T) \left(\frac{1}{1+\chi_S(T) H_{CB}(T)/M_r(T)} \right) \qquad \text{(Equation 5)}$$

where $\chi_S(T)$ is the superparamagnetic susceptibility given by $\chi_S(T) = \frac{25 M_S{}^2}{3KT} \int_0^T T_B f(T_B) dT_B$. Considering the experimental values of $f(T_B)$, shown in the insets of Figure 2, the temperature dependence of $\langle H_C \rangle_T$ was calculated with H_0 as the only free parameter. The full lines in Figure 3b show the fitting of the experimental data with Equation 5. Notice that, in spite of the complexity of the magnetization reversal process in bimagnetic core/shell NPs, we have obtained a good agreement because $f(T_B)$ includes overall terms that affect the energy barrier.[40] In the particular case of the ZnO/$CoFe_2O_4$ NPs we have added to the superparamagnetic susceptibility contribution $\chi_S(T)$ a second C/T term in order to account for the surface disorder contribution evidenced by the low temperature sharp decreasing of $M_S(T)$, where C = 0.05 emuKOe^{-1}cm^{-3} was obtained.

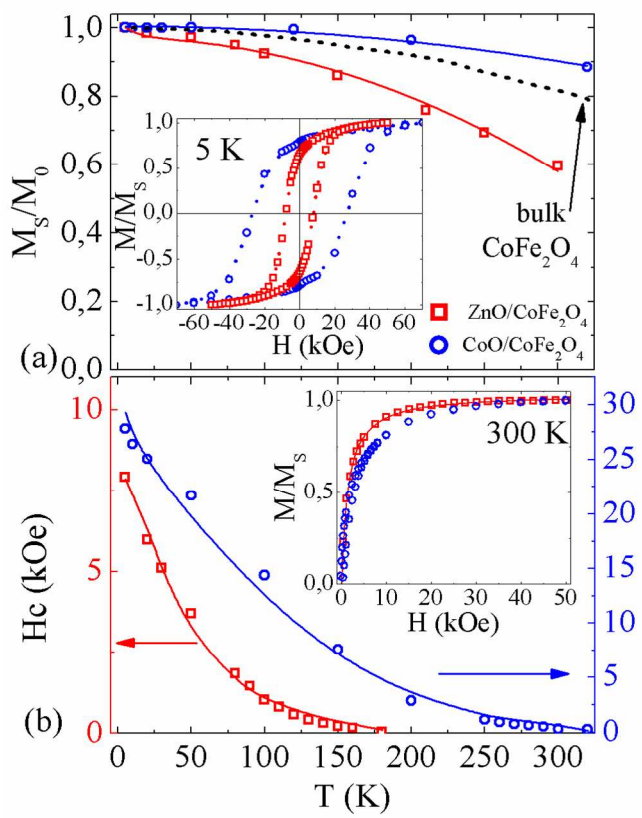

Figure 3 (a) Temperature dependence of the saturation magnetization ratio M_S/M_0 for $ZnO/CoFe_2O_4$ and $CoO/CoFe_2O_4$ nanoparticles (bulk $CoFe_2O_4$ experimental values from ref 41 are shown for comparison). Inset: Hysteresis loops at 5 K. (b) Temperature dependence of the coercive field. Inset: field dependence of magnetization at 300 K. (full lines represent the corresponding fits).

3.3 Intra- and inter-particle magnetic interactions

3.3.1 Remanent magnetization studies

Magnetization remanence experiments were conducted to get a better comprehension of the role of interactions.[42] The method consists in measuring an isothermal remanent magnetization curve (IRM) and a direct current demagnetization curve (DCD) from which information about interactions can be derived. By differentiating the remanence curves, a

field dependent irreversible susceptibility (χ_{irr}) can be calculated. $\chi_{irr}(H)$ is related to the distribution of coercive fields and, in NPs, it is associated to the energy barrier distribution.[25,42–44] Figures 4a-b show the IRM and DCD magnetization curves for $CoO/CoFe_2O_4$ and $ZnO/CoFe_2O_4$ NPs measured at 10 K and the insets show the corresponding χ_{irr}. Wohlfarth predicted that non-interacting single-domain particles with uniaxial anisotropy follow the relation $m_{DCD}(H) = 1 - 2m_{IRM}(H)$,[45] where m_{DCD} and m_{IRM} stand for the remanent magnetization divided by the saturation remanent magnetization in DCD and IRM curves, respectively. Deviations from the equation above would indicate the presence of different interactions that affect the energy barrier: if $\delta m(H) = m_{DCD}(H) - [1 - 2m_{IRM}(H)] < 0$, then demagnetizing interactions are dominant, whereas $\delta m(H) > 0$ implies the prevalence of magnetizing interactions.[46]

The δm plots for $CoO/CoFe_2O_4$ and $ZnO/CoFe_2O_4$ NPs measured at 10 K are shown in Figure 4c, both suggesting the presence of demagnetizing interactions. For $CoO/CoFe_2O_4$ NPs δm peak (ΔHp) is centered around 27 kOe, while for $ZnO/CoFe_2O_4$ NPs ΔHp is shifted to lower fields (around 9 kOe) in agreement with the lower anisotropy of the last system. The interactions strength can be assessed by comparing the $\chi_{irr}(H)$ curves obtained from DCD and IRM; the difference between H_{IRM} and H_{DCD} magnetic fields associated to the maximum of χ_{irr} curves is related to an interaction field given by $H_{int} = \frac{H_{DCD} - H_{IRM}}{2}$. The strength of the interactions was evaluated by calculating the H_{int}, which resulted to be -0.1 kOe and -0.9 kOe for the $ZnO/CoFe_2O_4$ and $CoO/CoFe_2O_4$ samples, respectively. Given the demagnetizing nature and magnitude of the calculated interacting fields we ascribe them to the inter-particle dipolar interaction. The smaller H_{int} value found for $ZnO/CoFe_2O_4$ could

be related to the smaller magnetic moment of the FiM shell due to the larger surface disorder as compared to the $CoO/CoFe_2O_4$ system.

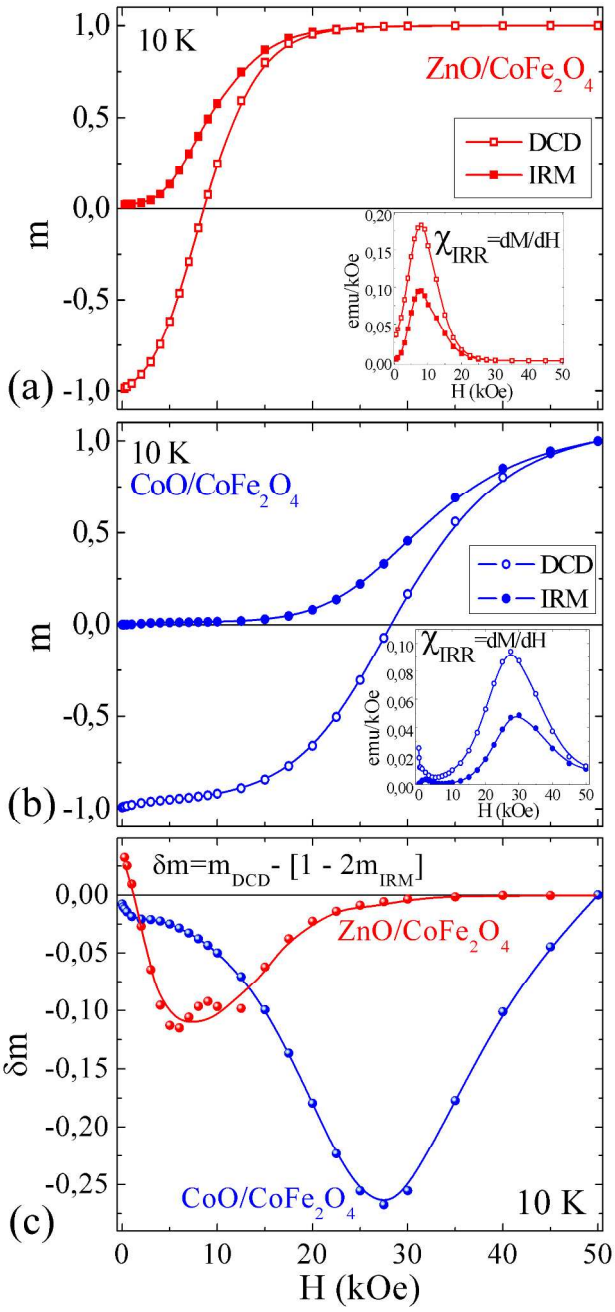

Figure 4 DCD (empty symbols) and IRM (full symbols) curves for (a) ZnO/CoFe2O4 nanoparticles and (b) CoO/CoFe2O4 nanoparticles measured at 10 K. (c) δm plots and

(insets) irreversible susceptibilities calculated from the DCD and IRM curves (lines are a guide to the eye).

3.3.2 Magnetic relaxation and activation volumes

A further insight in the reversal of magnetization can be attained by performing magnetic relaxation measurements. These experiments, mainly employed in the characterization of recording media to determine the stability of the stored information, have also been employed to study the time-dependent properties of permanent magnets.[47,48] Moreover, relaxation measurements provide information about the magnetization reversal and the origin of hysteretic behavior.[49–51] In NPs' systems, the time relaxation of the magnetization is originated by the thermally activated reversal of the magnetization against the energy barriers of the system. It is frequently described by the logarithmic decay given by Equation 6, where S denotes the magnetic viscosity coefficient, t is the time, t_0 is a reference time and $M(t_0)$ is the magnetization value at t_0,

$$M(t) = M(t_0) + Sln(t/t_0) \qquad \text{(Equation 6)}$$

The magnetic viscosity depends on the field at which the magnetization is recorded and tends to be maximum close to the coercive field, reflecting the link between S and the energy barrier distribution represented by $\chi_{irr}(H)$.[50] By measuring $M(t)$ at different applied fields (as shown in Figure S3) and fitting the results according to Equation 6 then $S(H)$ can be obtained as it is shown in Figure 5.

From the maximum values of $S(H)$ and $\chi_{irr}(H)$ a fluctuation field defined as $H_f = S^{MAX}/\chi_{irr}^{MAX}$ can be calculated.[44] H_f is related to the activation volume (V_{ACT}) where the magnetization reversal initiates through $V_{ACT} = k_B T/(M_S H_f)$.[50,52] V_{ACT} can be defined as the smallest volume of the material that reverses coherently in an event[53]. From the H_f

value obtained at 10 K we calculated the activation volume for both systems, that resulted to be 69(5) nm^3 and 46(6) nm^3 for $ZnO/CoFe_2O_4$ and $CoO/CoFe_2O_4$, respectively, as reported in Table 1. In the case of non-interacting single-domain NPs, the activation volume is equal to the particle size, however local effects tend to reduce V_{ACT}.[52] Considering the total $CoFe_2O_4$ shell volume V ~ 235 nm^3, which is similar for both systems, we found that the activation volume is three times smaller than V when the core is ZnO and five times smaller for the CoO case. The nucleation of magnetization reversal that defines the activation or switching field can be originated by local variations of anisotropy and structural disorder. Nucleation and interactions are competing processes[54] and, in this sense, the AFM-FiM coupling in $CoO/CoFe_2O_4$ is promoting a greater degree of incoherent rotation.[48]

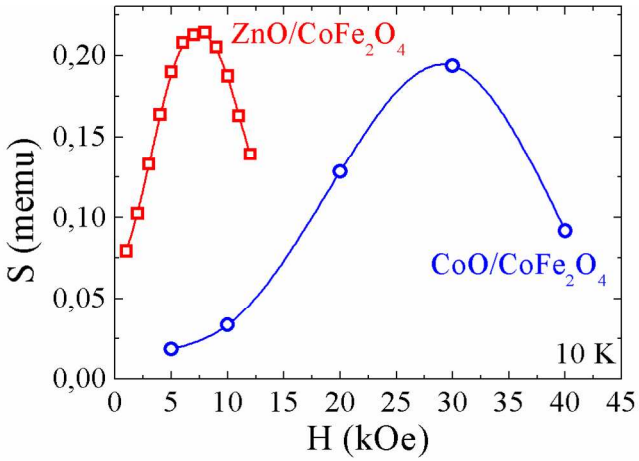

Figure 5 Magnetic viscosity coefficient (S) as a function of the reverse field for $ZnO/CoFe_2O_4$ and $CoO/CoFe_2O_4$ nanoparticles (lines are a guide to the eye).

In the Stoner-Wohlfarth model for non-interacting NPs with uniaxial anisotropy the activation volume can be calculated by $V_{ACT} = V\sqrt{\frac{25k_BT}{KV}}$ [50] where V denotes the physical volume and K the effective magnetic anisotropy. Such relationship can be rewritten in

terms of the mean blocking temperature as $V_{ACT} = V\sqrt{\frac{T}{\langle T_B \rangle}}$, then, the expected V_{ACT} can be simply derived from measured parameters. Such calculations lead to a V_{ACT} of 45(2) nm^3 and 72(3) nm^3 for CoO/$CoFe_2O_4$ and ZnO/$CoFe_2O_4$, respectively. It can be noted that the calculated V_{ACT} through the equation above and the measured V_{ACT} reported in Table 1 are in good agreement and come from independent measurements. Consequently, it seems clear that the smaller V_{ACT} found for CoO/$CoFe_2O_4$ is originated by the same mechanism that increases the thermal stability, *i.e.* the intra-particle interactions.

The strength of the intra-particle interaction can be estimated from the energy barrier. In the simplest model the energy barrier of the nanoparticle is originated by the contribution of different terms that account for the interactions of the system,

$$\Delta E = \Delta E_0 + \Delta E_{intra} + \Delta E_{inter} \quad \text{(Equation 7)}$$

where ΔE_0 arises from the magnetocrystalline, surface and shape anisotropy and ΔE_{intra}, ΔE_{inter} account for the intra-particle and inter-particle interactions respectively. In spite of the complexity of the magnetic systems (multiple energy minima, multi-domain particles) arising from the core/shell structure, Equation 7 simplifies the picture by considering the contributions of intra- and inter-particle interactions to an energy barrier in an Arrhenius thermal activated process. Assuming this approximation, from the Néel equation and the calculated mean blocking temperature we can estimate $\Delta E = 25 k_B \langle T_B \rangle$ for ZnO/$CoFe_2O_4$ and CoO/$CoFe_2O_4$ NPs. If we assume that ΔE_0 and ΔE_{inter} are similar for both systems, the differences between the energy barriers could be then explained by the intra-particle interactions, only present in CoO/$CoFe_2O_4$ due the interface exchange interaction. To compare the strength of such interactions we can associate an effective magnetic field to the

ΔE_{intra} through $\Delta E_{intra} \sim H_{intra} M_S V_{ACT}$. In this way, using the experimental V_{ACT} values and a $M_S \sim 80\ emu/g$, the intra-particle interaction field results to be $H_{intra} \sim 24\ kOe$. It is worth noting that the calculated interaction field is much larger than the interaction fields estimated from the remanence study (-0.1 kOe and -0.9 kOe for $ZnO/CoFe_2O_4$ and $CoO/CoFe_2O_4$ samples, respectively), supporting its exchange-coupling origin. Therefore, the remanence measurements allow to quantify the strength of dipolar inter-particle interactions of these systems but fail to account for the intra-particle interaction probably because of the strong coupling between the AFM and FiM phases and, according to ref 55, $\delta m(H)$ curve does not account for cooperative effects. These features are in agreement with a magnetization reversal process where the interface exchange interaction, J_{INT}, is much larger than the AFM anisotropy of the core ($J_{INT} \gg K_{AFM} V_{AFM}$) and, as a consequence, it is energetically more favorable for the spins in both FiM and AFM to rotate together.[56] This picture is consistent with the enhancement of the coercive field and the absence of exchange bias fields in the AFM-core/FiM-shell NPs.[23]

4. CONCLUSIONS

New bimagnetic nanoparticles systems have been proposed in the last years and their increasing complexity requires comprehensive magnetic studies in order to understand their properties. In this work, we have studied two core/shell magnetic systems, one formed by a diamagnetic core surrounded by ferrimagnetic $CoFe_2O_4$ and the other formed by an antiferromagnetic core surrounded by ferrimagnetic $CoFe_2O_4$. Since both systems present comparable size and morphology, from our studies some general issues about core/shell systems can be discussed. First, it is worth noting that core/shell NPs with a core that

occupies ~12 % of the total NP volume present magnetic properties that strongly depend on the magnetic nature of the core material and that are very different compared to single-phase particles of similar volume.

For the non-magnetic core the results can be interpreted by dominant surface effects induced into the ferrimagnetic phase by the shell morphology. The large magnetic surface disorder of the FiM shell is reflected in the M_S reduction with temperature and in the relatively low H_C compared to single-phase $CoFe_2O_4$ NPs, whose low-temperature H_C was found to be between 10 and 18 kOe.[57–60] In addition, viscosity measurements suggest that the activation or switching volume is nearly a third of the total shell volume, even if the total volume is lower than the critical single-domain volume. Such results evidence the importance of local effects, *e.g.* local structural and compositional inhomogeneities, on the reversal process.[54,61] On the contrary, the exchange interaction at the interface reduces the magnetic surface disorder in $CoO/CoFe_2O_4$ as it is reflected by the weak temperature dependence of the $M_S(T)$, in agreement with previous studies of the effects of interactions on the NPs' properties.[62] The magnetic behavior of $CoO/CoFe_2O_4$ NPs is governed by the intra-particle interactions that lead to an enhancement of the thermal stability and a magnetic hardening of the system. The strength of the intra-particle interactions estimated from the energy barrier is much larger than the interaction fields estimated from the remanence study supporting its exchange-coupling origin. Finally, by combining remanence and relaxation studies we have presented a direct measurement of how the exchange anisotropy in bimagnetic NPs rules the magnetization reversal by promoting a smaller switching volume, nearly a fifth of the total $CoFe_2O_4$ shell volume. Therefore the interface exchange coupling, apart from increasing the energy barrier, may be responsible for a greater degree of incoherent rotation.

In conclusion, to understand of how the static and dynamic energy landscape is related to the real structure of the material is important for the development of new artificial structures. The present study intends to clarify the determining role played by the morphology, the surface disorder, as well as the inter- and intra-particle interactions in the reversal magnetization process, and could orient future materials' development with tuned magnetic properties.

AUTHOR INFORMATION

Corresponding author

* E-mail: winkler@cab.cnea.gov.ar. Tel: +54-294-4445180

ACKNOWLEDGEMENTS

The authors thank ANPCyT Argentina through Grant PICT-2012-0492, CONICET Argentina through Grant PIP 112-20110100519, UNCuyo Argentina through Grants 06-C404 and C011, the Bilateral Project Argentina-CNR common projects 2013-2014 and the Joint Laboratory LIANAM.

ASSOCIATED CONTENT

Supporting Information

Temperature and time dependence of magnetization at different applied fields, for $ZnO/CoFe_2O_4$ and $CoO/CoFe_2O_4$ NPs and distributions of blocking temperatures at different applied fields for $CoO/CoFe_2O_4$ NPs. This information is available free of charge via the Internet at http://pubs.acs.org.

REFERENCES

(1) Sort, J.; Nogués, J.; Suriñach, S.; Muñoz, J. S.; Baró, M. D.; Chappel, E.; Dupont, F.; Chouteau, G. Coercivity and Squareness Enhancement in Ball-Milled Hard Magnetic–antiferromagnetic Composites. *Appl. Phys. Lett.* **2001**, *79*, 1142.

(2) Reiss, G.; Hütten, A. Magnetic Nanoparticles: Applications beyond Data Storage. *Nat. Mater.* **2005**, *4*, 725–726.

(3) Black, C. T.; Murray, C. B.; Sandstrom, R. L.; Sun, S. Spin-Dependent Tunneling in Self-Assembled Cobalt-Nanocrystal Superlattices. *Science* **2000**, *290*, 1131–1134.

(4) Dai, Q.; Berman, D.; Virwani, K.; Frommer, J.; Jubert, P.-O.; Lam, M.; Topuria, T.; Imaino, W.; Nelson, A. Self-Assembled Ferrimagnet--Polymer Composites for Magnetic Recording Media. *Nano Lett.* **2010**, *10*, 3216–3221.

(5) Liu, F.; Zhu, J.; Yang, W.; Dong, Y.; Hou, Y.; Zhang, C.; Yin, H.; Sun, S. Building Nanocomposite Magnets by Coating a Hard Magnetic Core with a Soft Magnetic Shell. *Angew. Chem. Int. Ed. Engl.* **2014**, *53*, 2176–2180.

(6) Zeng, H.; Li, J.; Liu, J. P.; Wang, Z. L.; Sun, S. Exchange-Coupled Nanocomposite Magnets by Nanoparticle Self-Assembly. *Nature* **2002**, *420*, 395–398.

(7) Balamurugan, B.; Sellmyer, D. J.; Hadjipanayis, G. C.; Skomski, R. Prospects for Nanoparticle-Based Permanent Magnets. *Scr. Mater.* **2012**, *67*, 542–547.

(8) Sort, J.; Suriñach, S.; Muñoz, J.; Baró, M.; Nogués, J.; Chouteau, G.; Skumryev, V.; Hadjipanayis, G. Improving the Energy Product of Hard Magnetic Materials. *Phys. Rev. B* **2002**, *65*, 174420.

(9) Liu, H.; Wu, J.; Min, J. H.; Zhang, X.; Kim, Y. K. Tunable Synthesis and Multifunctionalities of Fe_3O_4–ZnO Hybrid Core-Shell Nanocrystals. *Mater. Res. Bull.* **2013**, *48*, 551–558.

(10) Lu, A.-H.; Salabas, E. L.; Schüth, F. Magnetic Nanoparticles: Synthesis, Protection, Functionalization, and Application. *Angew. Chem. Int. Ed. Engl.* **2007**, *46*, 1222–1244.

(11) Gupta, A. K.; Gupta, M. Synthesis and Surface Engineering of Iron Oxide Nanoparticles for Biomedical Applications. *Biomaterials* **2005**, *26*, 3995–4021.

(12) Cho, N.-H.; Cheong, T.-C.; Min, J. H.; Wu, J. H.; Lee, S. J.; Kim, D.; Yang, J.-S.; Kim, S.; Kim, Y. K.; Seong, S.-Y. A Multifunctional Core-Shell Nanoparticle for Dendritic Cell-Based Cancer Immunotherapy. *Nat. Nanotechnol.* **2011**, *6*, 675–682.

(13) Nandwana, V.; Chaubey, G. S.; Yano, K.; Rong, C.; Liu, J. P. Bimagnetic Nanoparticles with Enhanced Exchange Coupling and Energy Products. *J. Appl. Phys.* **2009**, *105*, 014303.

(14) López-Ortega, A.; Tobia, D.; Winkler, E.; Golosovsky, I. V; Salazar-Alvarez, G.; Estradé, S.; Estrader, M.; Sort, J.; González, M. A.; Suriñach, S.; et al. Size-Dependent Passivation Shell and Magnetic Properties in Antiferromagnetic/ferrimagnetic Core/shell MnO Nanoparticles. *J. Am. Chem. Soc.* **2010**, *132*, 9398–9407.

(15) H. Zeng Z.L. Wang, J.P. Liu and S. Sun, J. L. Bimagnetic Core/Shell FePt/Fe_3O_4 Nanoparticles. *Nano Lett.* **2004**, *4*, 187–190.

(16) Lavorato, G. C.; Lima Jr, E.; Tobia, D.; Fiorani, D.; Troiani, H. E.; Zysler, R. D.; Winkler, E. L. Size Effects in Bimagnetic CoO/$CoFe_2O_4$ Core/shell Nanoparticles. *Nanotechnology* **2014**, *25*, 355704.

(17) Binns, C.; Qureshi, M. T.; Peddis, D.; Baker, S. H.; Howes, P. B.; Boatwright, A.; Cavill, S. A.; Dhesi, S. S.; Lari, L.; Kröger, R.; et al. Exchange Bias in Fe@Cr Core-Shell Nanoparticles. *Nano Lett.* **2013**, *13*, 3334–3339.

(18) Lima, E.; Winkler, E. L.; Tobia, D.; Troiani, H. E.; Zysler, R. D.; Agostinelli, E.; Fiorani, D. Bimagnetic CoO Core/$CoFe_2O_4$ Shell Nanoparticles: Synthesis and Magnetic Properties. *Chem. Mater.* **2012**, *24*, 512–516.

(19) Sun, X.; Huls, N. F.; Sigdel, A.; Sun, S. Tuning Exchange Bias in Core/shell FeO/Fe_3O_4 Nanoparticles. *Nano Lett.* **2012**, *12*, 246–251.

(20) Baaziz, W.; Pichon, B. P.; Lefevre, C.; Ulhaq-Bouillet, C.; Greneche, J.-M.; Toumi, M.; Mhiri, T.; Bégin-Colin, S. High Exchange Bias in $Fe_{3-\delta}O_4$@CoO Core Shell Nanoparticles Synthesized by a One-Pot Seed-Mediated Growth Method. *J. Phys. Chem. C* **2013**, *117*, 11436–11443.

(21) Sun, S.; Zeng, H. Size-Controlled Synthesis of Magnetite Nanoparticles. *J. Am. Chem. Soc.* **2002**, *124*, 8204–8205.

(22) Kwon, S. G.; Hyeon, T. Formation Mechanisms of Uniform Nanocrystals via Hot-Injection and Heat-up Methods. *Small* **2011**, *7*, 2685–2702.

(23) Winkler, E. L.; Lima, E.; Tobia, D.; Saleta, M. E.; Troiani, H. E.; Agostinelli, E.; Fiorani, D.; Zysler, R. D. Origin of Magnetic Anisotropy in ZnO/$CoFe_2O_4$ and CoO/$CoFe_2O_4$ Core/shell Nanoparticle Systems. *Appl. Phys. Lett.* **2012**, *101*, 252405.

(24) Lavorato, G. C.; Lima, E.; Troiani, H. E.; Zysler, R. D.; Winkler, E. L. Exchange-Coupling in Thermal Annealed Bimagnetic Core/shell Nanoparticles. *J. Alloys Compd.* **2015**, *633*, 333–337.

(25) Dormann, J. L.; Fiorani, D.; Tronc, E. *Magnetic Relaxation in Fine-Particle Systems. Advanced in Chemical Physics Vol XCVIII*; Wiley: New York, 1997.

(26) Peddis, D.; Cannas, C.; Musinu, A.; Ardu, A.; Orrù, F.; Fiorani, D.; Laureti, S.; Rinaldi, D.; Muscas, G.; Concas, G.; et al. Beyond the Effect of Particle Size: Influence of $CoFe_2O_4$ Nanoparticle Arrangements on Magnetic Properties. *Chem. Mater.* **2013**, *25*, 2005–2013.

(27) Chantrell, R. W.; El-Hilo, M.; O'Grady, K. Spin-Glass Behavior in a Fine Particle System. *IEEE Trans. Magn.* **1991**, *27*, 3570–3578.

(28) Dormann, J. L.; Fiorani, D.; El Yamani, M. Field Dependence of the Blocking Temperature in the Superparamagnetic Model: H2/3 Coincidence. *Phys. Lett. A* **1987**, *120*, 95–99.

(29) Nunes, W.; Socolovsky, L.; Denardin, J.; Cebollada, F.; Brandl, A.; Knobel, M. Role of Magnetic Interparticle Coupling on the Field Dependence of the Superparamagnetic Relaxation Time. *Phys. Rev. B* **2005**, *72*, 212413.

(30) M. El-Hilo, K. O. and R. W. C. Susceptibility Phenomena in a Fine Particle System. *J. Magn. Magn. Mater.* **1992**, *114*, 307–313.

(31) Peddis, D.; Rinaldi, D.; Ennas, G.; Scano, a.; Agostinelli, E.; Fiorani, D. Superparamagnetic Blocking and Superspin-Glass Freezing in Ultra Small Δ-(Fe0.67Mn0.33)OOH Particles. *Phys. Chem. Chem. Phys.* **2012**, *14*, 3162.

(32) Chantrell, R.; Popplewell, J.; Charles, S. Measurements of Particle Size Distribution Parameters in Ferrofluids. *IEEE Trans. Magn.* **1978**, *14*, 975–977.

(33) Cullity, B. D.; Graham, C. D. *Introducion to Magnetic Materials*; 2nd ed.; John Wiley & Sons: New Jersey, 2009.

(34) Kodama, R. H. Magnetic Nanoparticles. *J. Magn. Magn. Mater.* **1999**, *200*, 359–372.

(35) Hendriksen, P. V; Linderoth, S.; Lindgard, P. Magnetic Properties of Heisenberg Clusters. *J. Phys. Condens. Matter* **1993**, *5*, 5675–5684.

(36) Vázquez-Vázquez, C.; López-Quintela, M. a.; Buján-Núñez, M. C.; Rivas, J. Finite Size and Surface Effects on the Magnetic Properties of Cobalt Ferrite Nanoparticles. *J. Nanoparticle Res.* **2010**, *13*, 1663–1676.

(37) McDannald, A.; Staruch, M.; Jain, M. Surface Contributions to the Alternating Current and Direct Current Magnetic Properties of Oleic Acid Coated $CoFe_2O_4$ Nanoparticles. *J. Appl. Phys.* **2012**, *112*, 123916.

(38) Nunes, W.; Folly, W.; Sinnecker, J.; Novak, M. Temperature Dependence of the Coercive Field in Single-Domain Particle Systems. *Phys. Rev. B* **2004**, *70*, 014419.

(39) Kneller, E. F.; Luborsky, F. E. Particle Size Dependence of Coercivity and Remanence of Single-Domain Particles. *J. Appl. Phys.* **1963**, *34*, 656–658.

(40) Curiale, J.; Sánchez, R.; Troiani, H.; Ramos, C.; Pastoriza, H.; Leyva, a.; Levy, P. Magnetism of Manganite Nanotubes Constituted by Assembled Nanoparticles. *Phys. Rev. B* **2007**, *75*, 224410.

(41) Shenker, H. Magnetic Anisotropy of Cobalt Ferrite ($Co_{1.01}Fe_{2.00}O_{3.62}$) and Nickel Cobalt Ferrite ($Ni_{0.72}Fe_{0.20}Co_{0.08}Fe_2O_4$). *Phys. Rev.* **1957**, *107*, 1246–1249.

(42) Binns, C. *Nanomagnetism: Fundamentals and Applications*; Frontiers of Nanoscience; Elsevier Science, 2014.

(43) O'Grady, K.; El-Hilo, M.; Chantrell, R. W. The Characterisation of Interaction Effects in Fine Particle Systems. *IEEE Trans. Magn.* **1993**, *29*, 2608–2613.

(44) Laureti, S.; Varvaro, G.; Testa, A. M.; Fiorani, D.; Agostinelli, E.; Piccaluga, G.; Musinu, A.; Ardu, A.; Peddis, D. Magnetic Interactions in Silica Coated Nanoporous Assemblies of $CoFe_2O_4$ Nanoparticles with Cubic Magnetic Anisotropy. *Nanotechnology* **2010**, *21*, 315701.

(45) Wohlfarth, E. P. Relations between Different Modes of Acquisition of the Remanent Magnetization of Ferromagnetic Particles. *J. Appl. Phys.* **1958**, *29*, 595.

(46) Kelly, P. E.; O'Grady, K.; Mayo, P. I.; Chantrell, R. W. Switching Mechanisms in Cobalt-Phosphorus Thin Films. *IEEE Trans. Magn.* **1989**, *25*, 3881–3883.

(47) Street, R.; Woolley, J. C. A Study of Magnetic Viscosity. *Proc. Phys. Soc. Sect. A* **1949**, *62*, 562–572.

(48) Chantrell, R. Magnetic Viscosity of Recording Media. *J. Magn. Magn. Mater.* **1991**, *95*, 365–378.

(49) Antonel, P. S.; Negri, R. M.; Leyva, A. G.; Jorge, G. A. Anisotropy and Relaxation Processes of Uniaxially Oriented $CoFe_2O_4$ Nanoparticles Dispersed in PDMS. *Phys. B Condens. Matter* **2012**, *407*, 3165–3167.

(50) Bertotti, G. *Hysteresis in Magnetism: For Physicists, Materials Scientists, and Engineers*; Academic Press series in electromagnetism; Academic Press, 1998.

(51) Butera, A.; Weston, J. L.; Barnard, J. A. Activation Volumes and Interparticle Interaction Effects in Nanostructured Fe Networks. *J. Appl. Phys.* **1997**, *81*, 7432.

(52) Patel, V.; EL-Hilo, M.; O'Grady, K.; Chantrell, R. W. Nucleation Fields in an Exchange Spring Hard Magnet. *J. Phys. D. Appl. Phys.* **1993**, *26*, 1453–1458.

(53) O'Grady, K.; Laidler, H. The Limits to Magnetic Recording - Media Considerations. *J. Magn. Magn. Mater.* **1999**, *200*, 616–633.

(54) Skomski, R. Nanomagnetics. *J. Phys. Condens. Matter* **2003**, *15*, R841–R896.

(55) Skomski, R.; Sellmyer, D. J. Cooperative Magnetism and the Preisach Model. *J. Appl. Phys.* **2001**, *89*, 7263–7265.

(56) Nogués, J.; Schuller, I. K. Exchange Bias. *J. Magn. Magn. Mater.* **1999**, *192*, 203–232.

(57) Vestal, C. R.; Song, Q.; Zhang, Z. J. Effects of Interparticle Interactions upon the Magnetic Properties of $CoFe_2O_4$ and $MnFe_2O_4$ Nanocrystals. *J. Phys. Chem. B* **2004**, *108*, 18222–18227.

(58) Pianciola, B. N.; Lima, E.; Troiani, H. E.; Nagamine, L. C. C. M.; Cohen, R.; Zysler, R. D. Journal of Magnetism and Magnetic Materials Size and Surface Effects in the Magnetic Order of $CoFe_2O_4$ Nanoparticles. *J. Magn. Magn. Mater.* **2015**, *377*, 44–51.

(59) Peddis, D.; Orrù, F.; Ardu, A.; Cannas, C.; Musinu, A.; Piccaluga, G. Interparticle Interactions and Magnetic Anisotropy in Cobalt Ferrite Nanoparticles: Influence of Molecular Coating. *Chem. Mater.* **2012**, *24*, 1062–1071.

(60) Cannas, C.; Musinu, A.; Piccaluga, G.; Fiorani, D.; Peddis, D.; Rasmussen, H. K.; Mørup, S. Magnetic Properties of Cobalt Ferrite-Silica Nanocomposites Prepared by a Sol-Gel Autocombustion Technique. *J. Chem. Phys.* **2006**, *125*, 164714.

(61) Zeng, H.; Skomski, R.; Menon, L.; Liu, Y.; Bandyopadhyay, S.; Sellmyer, D. Structure and Magnetic Properties of Ferromagnetic Nanowires in Self-Assembled Arrays. *Phys. Rev. B* **2002**, *65*, 1–8.

(62) Winkler, E.; Zysler, R.; Fiorani, D. Surface and Magnetic Interaction Effects in Mn_3O_4 Nanoparticles. *Phys. Rev. B* **2004**, *70*, 174406.

TABLE OF CONTENTS GRAPHICS